

# HERS Superpixels: Deep Affinity Learning for Hierarchical Entropy Rate Segmentation

Hankui Peng<sup>1</sup>, Angelica I. Aviles-Rivero<sup>1</sup>, and Carola-Bibiane Schönlieb<sup>1</sup>

<sup>1</sup>DAMTP, University of Cambridge.  
{hp467, ai323, cbs31}@cam.ac.uk

## Abstract

*Superpixels serve as a powerful preprocessing tool in many computer vision tasks. By using superpixel representation, the number of image primitives can be largely reduced by orders of magnitudes. The majority of superpixel methods use handcrafted features, which usually do not translate well into strong adherence to object boundaries. A few recent superpixel methods have introduced deep learning into the superpixel segmentation process. However, none of these methods is able to produce superpixels in near real-time, which is crucial to the applicability of a superpixel method in practice. In this work, we propose a two-stage graph-based framework for superpixel segmentation. In the first stage, we introduce an efficient Deep Affinity Learning (DAL) network that learns pairwise pixel affinities by aggregating multi-scale information. In the second stage, we propose a highly efficient superpixel method called Hierarchical Entropy Rate Segmentation (HERS). Using the learned affinities from the first stage, HERS builds a hierarchical tree structure that can produce any number of highly adaptive superpixels instantaneously. We demonstrate, through visual and numerical experiments, the effectiveness and efficiency of our method compared to various state-of-the-art superpixel methods.*

## 1. Introduction

Superpixel segmentation is the task of partitioning an image into meaningful regions within which the pixels share similar qualities such as colour, texture, or other low-level features. Superpixel segmentation is a powerful preprocessing tool for many computer vision tasks. For example, image classification [5, 29], optical flow [25, 20], object tracking [38, 41] and semantic segmentation [15, 46]. Superpixels offer more computationally digestible input data representations than the conventional pixel-level format. By us-

ing superpixel representations, one can substantially reduce the number of primitives in an image, whilst at the same time, highlighting the discriminative information [1].

The aforementioned advantages have encouraged the fast advancement of superpixel segmentation techniques (e.g. [16, 1, 19, 17, 23, 36]) since the seminal work of Ren and Malik [28]. For a superpixel segmentation method to be useful, it should be computationally efficient and preserve the structure of the objects well (i.e. adhere to the object boundaries). Although the body of literature has reported promising results based on various schemes, the majority of existing works rely on hand-crafted features. This design choice limits the generalisability of superpixels across various types of scenes.

With the advent of deep learning, it becomes possible to explore more flexible representations in various superpixel segmentation techniques. However, to the best of our knowledge, there are only a few attempts to employ deep networks for superpixels (e.g. [34, 13, 42]). There are several reasons for this limited adoption. Firstly, the conventional convolution operation in a neural network is designed to work efficiently with a regular image grid, whereas superpixel segmentations naturally give rise to irregular grids. Secondly, there does not exist ground truth superpixels in an image, but rather a delineation of the object structure. Thirdly, several existing superpixel techniques (e.g. [1, 19]) are non-differentiable, due to the nearest neighbour assignment used in the pixel-superpixel association. This imposes a challenge in the network training process which would be end-to-end trainable otherwise.

So far, there are only a few works that have addressed the aforementioned challenges in integrating deep networks within superpixel methods. One possible approach is to redesign a network architecture to allow the computation of irregular superpixel grids, e.g. [8, 32, 42]. This is still challenging, particularly, if one wishes to integrate subsequent tasks within a single learning process. An alternative

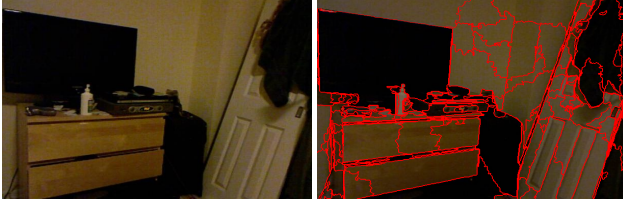


Figure 1: HERS produces superpixels that are highly adaptive to the homogeneous regions of an image. **Left:** the original image. **Right:** segmentation by DAL-HERS.

approach is to decouple the superpixel segmentation process from the deep network training process. For example, one can use a network to extract pixel-level features and then feed them into a superpixel segmentation method [13]. Most of these existing attempts are based on building upon a modified version of SLIC [1], which is based on Lloyd’s algorithm for  $k$ -means clustering, for its efficiency and simplicity. However, SLIC has a few limitations, such as the over-partition in homogeneous regions of an image and high computational cost in texture-rich regions.

As an alternative to clustering-based techniques, a number of researchers have demonstrated the potential of graph-based superpixel techniques [28, 34]. Under this framework, the superpixel segmentation task is translated into a graph partitioning one. The key challenge in this framework lies in obtaining a good partition of the graph. In addition, the problem of learning pixel-wise affinities from a standard deep network that can translate well into edge weights of a graph is not trivial. With that said, the graph-based framework provides several advantages such as computational tractability, natural representation of an image, and desirable tree structure.

In this work, we present a two-stage graph-based superpixel segmentation framework, where an output example is displayed in Figure 1. In the first stage, we propose a deep network structure, Deep Affinity Learning (DAL), to learn pixel-wise affinities that are aware of the object boundaries. In the second stage, we propose an efficient graph partitioning method called Hierarchical Entropy Rate Segmentation (HERS). HERS produces highly adaptive superpixels that adhere well to the object boundaries whilst maximising the entropy rate of the resulting graph partition. To summarise, our main contributions are:

- We propose a deep network named DAL which learns and aggregates multi-scale information from an image, produces boundary-aware affinities, and can be trained efficiently.
- We propose an efficient superpixel segmentation algorithm called HERS that produces highly adaptive superpixels. Most importantly, HERS builds a hierarchical tree structure which allows any number of super-

pixels to be generated instantaneously.

- We evaluate our proposal on superpixel benchmark datasets that contain a range of indoor and outdoor scenes. Extensive experimental results demonstrate the effectiveness (numerically and visually) and efficiency of our proposal, which compares favourably against various state-of-the-art classical and deep learning based superpixel methods.

## 2. Related Work

Superpixel segmentation methods have been extensively studied in the literature, with the majority of existing techniques designed from the classical perspective. Most recently, a few works have reported the use of deep networks for superpixels. We review the existing techniques in turn.

**Classic Techniques for Superpixels.** Since the pioneering work of [28], several techniques have been proposed which can be roughly divided into patch-based models [7, 33], watershed techniques [9, 4, 22], clustering-based approaches [1, 17, 21, 2, 23, 44] and graph-based techniques [28, 6, 19, 12]. The last two categories are the most widely applied family of techniques, which we will cover in the rest of this section.

A set of techniques have been proposed based on clustering principles for superpixels. The most popular technique in this category is the Simple Linear Iterative Clustering (SLIC) [1]. This technique partitions a given image using a local version of the  $k$ -means algorithm. Whilst this technique offers simplicity and efficiency, it has several drawbacks. For example, it unnecessarily partitions uniform areas and computes unnecessary distances in dense areas. These issues motivated several improvements for  $k$ -means based techniques including reducing the number of distance calculations, improving the seeding initialisation and improving the feature representation [21, 17, 2, 23, 45].

Another set of techniques treat superpixel segmentation as a graph partitioning problem. The seminal paper of [28] uses the Normalised Cuts algorithm, where superpixels are subgraphs that are obtained as a result of the partitioning based on edge similarities. This technique produced fair results, with the boundary adherence being the main issue. Another graph based technique was presented in [6], where the main criterion for graph partitioning is based on the evidence for a boundary between two regions. The evidence relies on the intensity difference firstly on the boundaries and secondly between neighbouring pixels. This work inspired several other techniques such as the one in [39], where the weights on the graph are being adjusted iteratively. One of the most competitive graph-based techniques is Entropy Rate Superpixel Segmentation (ERS) which is first introduced in [19]. This technique considers edge weights as transition probabilities of a random walk, and

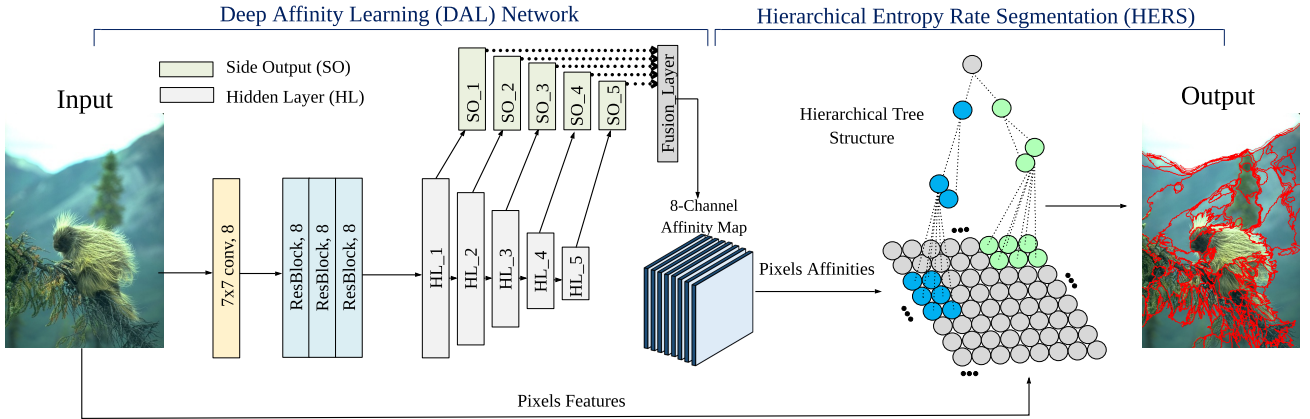


Figure 2: Illustration of our proposed superpixel framework. The left side of the scheme shows the flow of our proposed DAL network, which learns an 8-channel pixel affinity map. The right side displays our proposed HERS algorithm, which constructs a hierarchical tree structure that allows any number of highly adaptive superpixels to be generated instantaneously.

selects edges to form a number of subgraphs / superpixels that maximises the overall entropy rate of the partition. The problem is solved through a lazy greedy algorithm [27], which is not very computationally efficient. Several previous techniques, e.g. [10, 37, 45, 18, 30, 12], serve as the basis for other graph-based techniques.

**Deep Learning Techniques for Superpixels.** A commonality of classical techniques for superpixels is the use of hand-crafted features, which limits their generalisability. Whilst this problem has been addressed through the use of deep networks in many other computer vision tasks, this is not the case for superpixel segmentation where only a few works have been reported that employ deep networks. The application of deep learning has been formally introduced in the context of superpixels in [13]. The authors proposed the SSN model that uses a deep network to extract pixel-level features, and then use the learned features as input to a soft version of SLIC [1]. The key idea is to enforce soft-associations between pixels and superpixels to avoid the non-differentiability of SLIC. The authors of [34] introduced a graph-based model, where the key idea is to learn the pixel affinities for superpixel segmentation. This work is built upon ERS [19] along with a segmentation-aware loss. Most recently, [42] uses fully convolutional network in an Encoder-Decoder structure to learn the association between pixels and superpixels on a regular image grid.

**Distinctions in Our Approach.** Our technique is close in philosophy to that of [34] and [19]. Motivated by the graph principles, both our work and [34] seek to learn pixel-wise affinities. However, our proposal has several major advantages. Firstly, the work of [34] is limited by its own design – as it only allows the learning of pairwise pixel

affinities for one direction at a time. Therefore, the network needs to be applied twice to obtain both horizontal and vertical pixel affinities, which results only in a 4-connected affinity map. By contrast, our work learns a richer 8-connected affinity map within one training process. Secondly, the loss design of [34] requires applying a superpixel segmentation method for each training epoch. Additionally, it requires incorporating external edge information, which does not necessarily generalise well on the training set. In comparison, our work efficiently enforces boundary adherence by learning directly from the network without the need for superpixel segmentation or incorporation of external edge information throughout training. Finally, we introduce an efficient graph-based technique called Hierarchical Entropy Rate Segmentation (HERS). Unlike ERS [19], HERS is a parameter-free technique that produces adaptive superpixels whilst enforcing balanced cluster sizes. Notably, we offer a computational complexity of  $\mathcal{O}(|\mathcal{V}|)$ , as opposed to  $\mathcal{O}(|\mathcal{V}|^2 \log(|\mathcal{V}|))$  [19].

### 3. The Proposed Methodology

In this section, we present the two core parts of our proposed graph-based superpixel segmentation framework: i) our proposed **Deep Affinity Learning (DAL)** neural network architecture for obtaining deeply learned pixel affinities, and ii) our proposed **Hierarchical Entropy Rate Segmentation (HERS)** algorithm. An overview of our technique is displayed in Figure 2.

#### 3.1. Deeply Learned Affinities

In the first stage of our proposed framework, our goal is to design an effective and efficient network training scheme

that produces an 8-connected affinity map  $A \in \mathbb{R}^{8 \times H \times W}$  for any input image of height  $H$  and width  $W$ . The total number of pixels in an image is given by  $N = W \times H$ . For each pixel  $\mathbf{p}_i$ , we compute the affinities between  $\mathbf{p}_i$  and a maximum of 8 surrounding pixels that lie in its closest neighbourhood  $\mathcal{N}_i$ .

**Network design.** Our proposed Deep Affinity Learning network, DAL for short, consists of two parts. In the first part of the network, a  $7 \times 7$  convolutional kernel is used in the first layer to capture both the horizontal and vertical changes in an image. This is followed by 3 standard residual blocks [11] with 8 channels for producing an intermediate affinity map. In the second part of the network, we seek to enforce the preservation of fine details and scene structures. To achieve this, we integrate the HED network structure from [40]. That is, we incorporate five continuous blocks of layers which capture neighbourhood information at various scales. Each of these blocks outputs a side layer which are then concatenated at the end to produce the final 8-channel affinity map  $A$ .

**Loss function.** The training loss can be quantified separately for both boundary pixels and non-boundary pixels. The most common way of measuring the loss between the learned affinity map  $A$  and the ground truth segmentation map  $T \in \{0, 1\}^{8 \times H \times W}$  is through the following Binary Cross Entropy (BCE) loss:

$$\begin{aligned} \mathcal{L}_{BCE}(A, T) = & -\frac{1}{8N} \sum_{i=1}^N \sum_{j \in \mathcal{N}_i} (1 - t_{ij}) \log(1 - a_{ij}) \\ & -\frac{1}{8N} \sum_{i=1}^N \sum_{j \in \mathcal{N}_i} t_{ij} \log(a_{ij}), \end{aligned} \quad (1)$$

where  $t_{ij} \in \{0, 1\}$  denotes the ground truth relationship between pixel  $\mathbf{p}_i$  and  $\mathbf{p}_j$ , and  $a_{ij} \in [0, 1]$  denotes the learned affinity between pixel  $\mathbf{p}_i$  and  $\mathbf{p}_j$ .

It can be seen that (1) encourages the learned affinities to be zeros for boundary pixels, and ones for non-boundary pixels. However, the ground truth segmentations are often given for object detection instead of superpixel segmentation. Therefore, there is potentially no supervision information available in the heterogeneous regions within an object. Motivated by this, we propose the following modified version of (1):

$$\begin{aligned} \mathcal{L}_{DAL}(A, T) = & -\frac{1}{8N} \sum_{i=1}^N \sum_{j \in \mathcal{N}_i} (1 - t_{ij}) \cdot \log(1 - a_{ij}) \\ & -\frac{1}{8N} \sum_{i=1}^N \sum_{j \in \mathcal{N}_i} t_{ij} \cdot |g_{ij} - a_{ij}|, \end{aligned} \quad (2)$$

where  $w_{ij}$  denotes the pre-computed pairwise pixel affinity between  $\mathbf{p}_i$  and  $\mathbf{p}_j$ . We use the Gaussian similarity to

compute the pairwise pixel affinity  $g_{ij}$  as:

$$g_{ij} = -\exp\left(\frac{d(\mathbf{p}_i, \mathbf{p}_j)}{2\sigma^2}\right), \quad (3)$$

in which  $\sigma$  is the bandwidth parameter and  $d(\mathbf{p}_i, \mathbf{p}_j)$  denotes the distance between pixel  $\mathbf{p}_i$  and  $\mathbf{p}_j$ . It can be computed as the  $\ell_2$  distance between the RGB pixel features.

### 3.2. Hierarchical Entropy Rate Segmentation

After obtaining an 8-channel affinity map  $A \in \mathbb{R}^{8 \times H \times W}$  from our trained network, the second part of our proposed framework is to use the extracted rich information to generate superpixels. To achieve this, we introduce a technique called Hierarchical Entropy Rate Segmentation (HERS), which is detailed next.

The idea is to represent the extracted information as an undirected graph  $\mathcal{G} = (\mathcal{V}, \mathcal{E})$ , where  $\mathcal{V}$  denotes the set of nodes on the graph that correspond to the image pixels. The nodes in  $\mathcal{V}$  are connected by a set of edges  $\mathcal{E}$ , whose weights reflect the pairwise pixel similarities. The problem that we seek to solve is to select a subset of edges  $E \subset \mathcal{E}$  from the graph  $\mathcal{G} = (\mathcal{V}, \mathcal{E})$  such that the entropy rate of the segmentation is maximised. It has been shown in [19] that higher entropy rate corresponds to more compact and homogeneous clusters. The entropy rate is used to describe the uncertainty of a stochastic process. By modelling a graph  $\mathcal{G} = (\mathcal{V}, \mathcal{E})$  as a first-order Markov process, we can obtain the entropy rate of the graph as a conditional entropy.

In this framework, the transition probability between a pair of nodes  $v_i$  and  $v_j$  can be expressed as  $p_{ij} = w_{ij}/w_i$ , in which  $w_i = \sum_{k: e_{ik} \in \mathcal{E}} w_{ik}$  denotes the sum of edge weights connecting to node  $v_i$ . Here  $w_{ij}$  denotes the pairwise similarity between  $v_i$  and  $v_j$ , which can be readily obtained from the affinity map  $A$  as  $(a_{ij} + a_{ji})/2$ . A stationary distribution of the Markov process can be given as follows:

$$\boldsymbol{\mu} = [\mu_1, \mu_2, \dots, \mu_{|\mathcal{V}|}] = \left[ \frac{w_1}{w_T}, \frac{w_2}{w_T}, \dots, \frac{w_{|\mathcal{V}|}}{w_T} \right]^T. \quad (4)$$

Then the entropy rate of the graph can be expressed as

$$\mathcal{H}(\mathcal{E}) = -\sum_i \frac{w_i}{w_T} \sum_j \frac{w_{ij}}{w_i} \log \frac{w_{ij}}{w_i}, \quad (5)$$

where  $w_T = \sum_{i=1}^{|\mathcal{V}|} w_i$  denotes the sum of weights across all nodes. Our goal is to sequentially select edges, guided by the entropy rate criterion in (5), in order to *form balanced superpixels that are adaptive in sizes*. To do this, we propose to use Borůvka's algorithm to optimise solely the entropy rate of the graph, whilst obtaining balanced and adaptive superpixels.

Borůvka's algorithm is one of the oldest algorithms designed to identify the minimum spanning tree (MST) of a

graph  $\mathcal{G} = (\mathcal{V}, \mathcal{E})$ . It simultaneously goes through the following steps for all currently formed trees in the graph: i) identify the best edge for each tree, which consists of one node or a set of nodes that are already connected by existing edges, and ii) add those identified edges to the forest until one minimum spanning tree is formed connecting all nodes in the graph. Borůvka’s algorithm enjoys a number of desirable properties. Firstly, instead of having to sort all the edges globally as in the lazy greedy algorithm adopted by [19], Borůvka’s algorithm finds the best edges for all trees simultaneously. As a result, we can offer a computational complexity of  $\mathcal{O}(|\mathcal{V}|)$ , as opposed to  $\mathcal{O}(|\mathcal{V}|^2 \log(|\mathcal{V}|))$  as in [19]. In addition, the parallel edge selection process in Borůvka’s algorithm allows for the generation of very balanced trees. Finally, by recording the orders in which the edges are added, a hierarchical structure can be formed which allows any number of trees to be generated instantaneously. An illustration of these advantages is displayed in Figure 3.

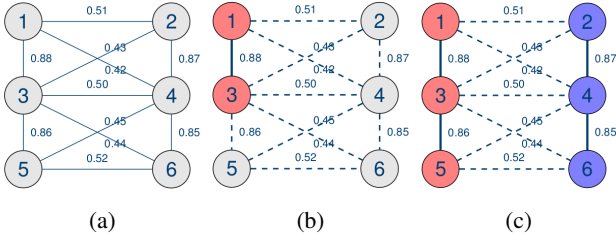


Figure 3: A simple example that illustrates the efficiency and parallelisability of Borůvka’s algorithm. It only needs one iteration to arrive at the final partitioning, whereas the lazy greedy algorithm in [19] requires four iterations.

The idea of using Borůvka’s algorithm for the purpose of superpixel segmentation has been previously utilised in [39]. However, [39] considers edge weights as dissimilarities between pairs of nodes, whereas we associate edge weights with their potential contributions to the overall entropy rate of the graph. Concretely, the edge weight can be interpreted in terms of its contribution to the overall entropy rate of the graph, if it were to be added to the current set of selected edges  $E$ . Using the learned affinities  $a_{ij} \in \mathcal{A}$  for the edge weight  $w_{ij}$  between node  $v_i$  and  $v_j$ , the edge weight  $w_{ij}$  can be calculated as:

$$\begin{aligned}
 w_{ij} &= \mathcal{H}(E \cup \{e_{ij}\}) - \mathcal{H}(E) \\
 &= (w_{ij} + \mu_i) \log(w_{ij} + \mu_i) + (w_{ij} + \mu_j) \log(w_{ij} + \mu_j) \\
 &\quad - \mu_i \log \mu_i - \mu_j \log \mu_j - 2w_{ij} \log w_{ij}.
 \end{aligned} \tag{6}$$

We refer to our proposal of sequential edge selection guided by entropy rate via Borůvka’s algorithm as **Hierarchical Entropy Rate Segmentation (HERS)**. The algorithmic form of HERS is presented in Algorithm 1. Note

---

### Algorithm 1: HERS Superpixels

---

```

Input: Graph:  $\mathcal{G} = (\mathcal{V}, \mathcal{E})$ 
1 Output: A minimum spanning tree  $T$ ; A set of
   selected edges  $E \subset \mathcal{E}$ 
2 Constructed tree:  $T = \emptyset$ ; Selected edges:  $E = \emptyset$ ;
   Unselected edges:  $U = \mathcal{E}$ 
3 function Borůvka( $\mathcal{G} = (\mathcal{V}, \mathcal{E})$ )
4   do
5     - Identify the currently formed trees
        $T_1, T_2, \dots, T_k$  where  $k \leq |\mathcal{V}|$ 
6     - Find the best outgoing edge for each tree
        $T_i$  ( $i = 1, 2, \dots, k$ ):
       
$$e^*(T_i) = \arg \max_{e_{ij} \in U_i} \mathcal{H}(E \cup \{e_{ij}\}) - \mathcal{H}(E),$$

       where  $U_i$  denotes the unselected outgoing
       edges for tree  $T_i$ 
7     - Sort the best outgoing edges in descending
       order:  $e^*(T_1), e^*(T_2), \dots, e^*(T_k)$ 
8     for  $\ell = 1, \dots, k$  do
9       Add the  $\ell$ -th outgoing edge to  $E$ ;
10       $K \leftarrow K - 1$ ;
11     end
12   while  $|T| > 1$ ;
13 end

```

---

that the number of superpixels  $K$  is not necessarily required as an input to the algorithm. Instead, a segmentation with any number of superpixels can be obtained instantaneously from the hierarchy that is constructed via Algorithm 1.

## 4. Experimental Results

In this section, we describe in detail the range of experiments that we conducted to demonstrate the effectiveness and efficiency of our proposed methodology.

**Dataset Description & Evaluation Protocol.** We evaluate the performance of our technique using two benchmark datasets for superpixels. We use The Berkeley Segmentation Dataset 500 (BSDS500) [3]. This dataset contains 500 images with provided ground truth segmentations. It provides a wide variety of outdoor scenes with different complex structures. We also use the NYU Depth Dataset V2 (NYUv2) [31], which consists of 1449 images with provided ground truth segmentations. The NYUv2 dataset provides a range of different indoor scenes.

We first justify the model design and support the advantage of our technique through a set of ablation studies. We then compare our technique with the following state-of-the-art techniques: i) classic techniques: ERS [19], SH [39], SLIC [1], SNIC [2], SEEDS [35], ETPS [43]; and

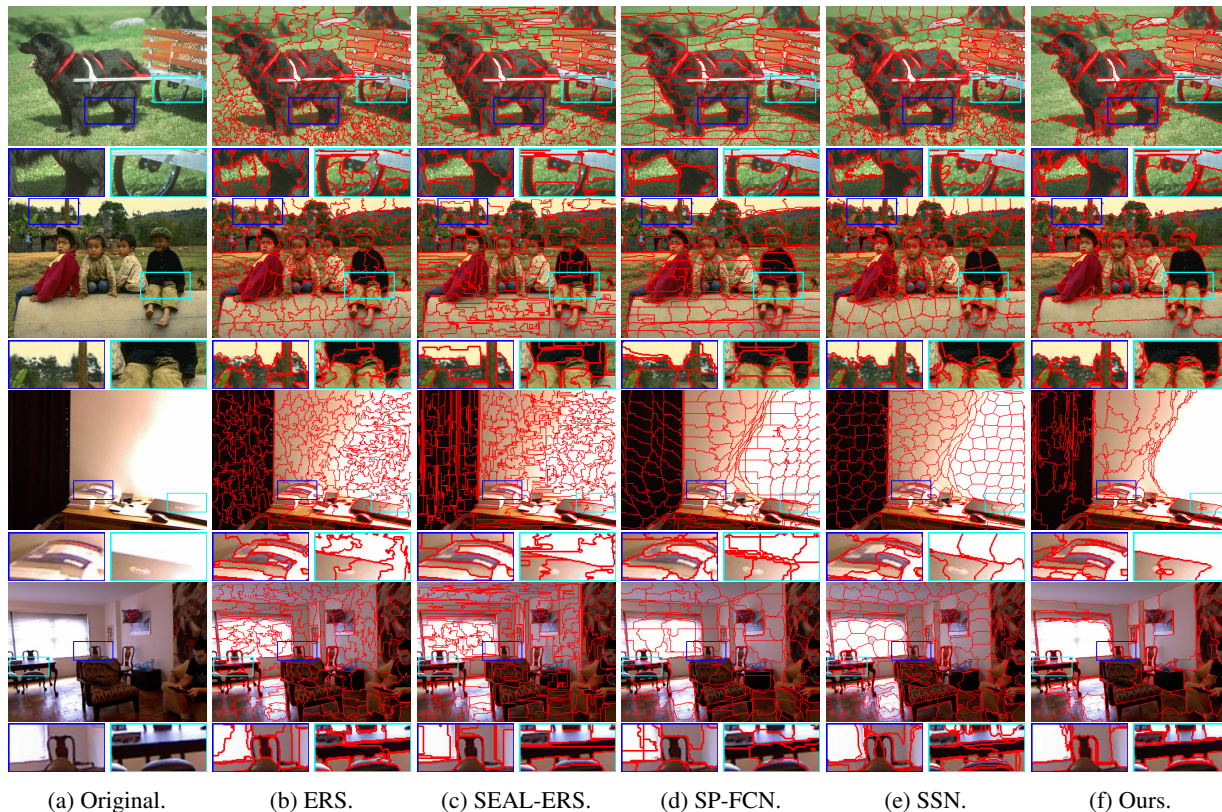


Figure 4: Visual comparison of our technique against a number of state-of-the-art algorithms using 200 superpixels. The selected images show variations in scenes from BSDS500 and NYUv2 datasets. We highlight some regions in the zoom-in views, where our technique better captures the fine details and enjoys strong boundary adherence whilst avoiding partitioning homogeneous areas.

ii) deep learning techniques: SSN [13], SEAL-ERS [34] and SP-FCN [42]. The most commonly used performance measures for evaluating superpixel segmentation algorithms include: Under-segmentation Error (UE) [35], Achievable Segmentation Accuracy (ASA) [19] and Boundary Recall (BR) [24]. In particular, UE can be directly obtained from ASA as  $1 - \text{ASA}$ . Thus, we report the ASA and BR measures in our experiments. Additionally, we also report the Explained Variation (EV) [26] that quantifies the variance within an image that is captured by the superpixels without relying on any ground truth labels. Explicit definitions of the metrics can be found in the supplementary material.

**Implementation & Training Details.** We learn an 8-channel affinity map by training our proposed DAL network on the BSDS500 training set. We implement the network in PyTorch using the Adam [14] optimiser with  $\beta_1 = 0.9$  and  $\beta_2 = 0.999$ . The DAL network is trained for 5k epochs, in which the input images are cropped to have size 200 by 200. The initial learning rate is set to  $1e - 4$ , and is reduced by a factor of 10 after 3k epochs. For all the competing methods, we use the code provided by the corresponding authors.

#### 4.1. Ablation Study

Our proposed methodology contains two main building blocks including the deeply learned affinities from the DAL network and the proposed HERS algorithm. In this section, we evaluate the contribution from each of these components. The comparison across different variants are reported in Figure 5 in terms of EV, BR, and ASA scores.

**Benefit of the proposed DAL network.** The benefit of using learned affinities from the DAL network as opposed to handcrafted ones can be observed by comparing the performance of ERS (green) with that of DAL-ERS (pink) in Figure 5. ERS computes the pixel-wise affinities using the Gaussian kernel in which the RGB pixel values are used as features. Whereas DAL-ERS directly uses the learned affinities from the DAL network as input to the ERS algorithm. It is clear that DAL-ERS (pink) largely outperforms the baseline ERS algorithm (green) in all three measures.

**Benefit of the proposed HERS algorithm.** Next, we inspect the contribution of our proposed superpixel segmentation algorithm HERS. It is worth pointing out that HERS does not require any balancing term in the objective func-

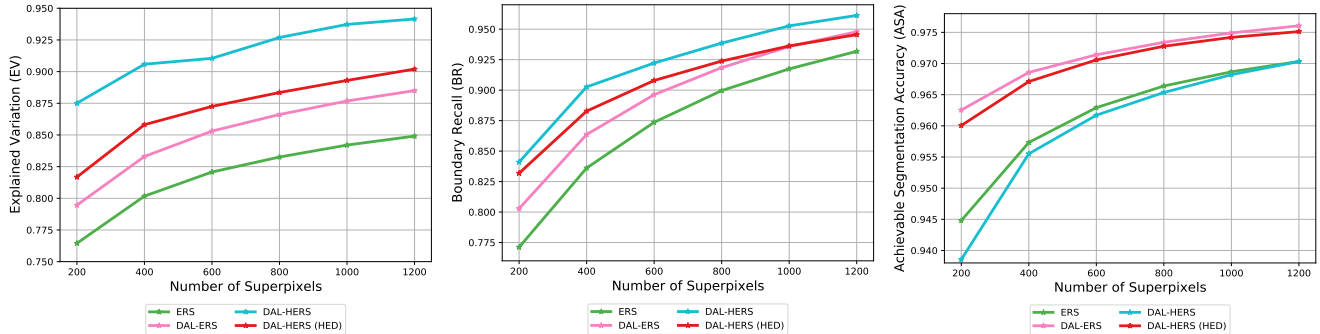


Figure 5: **Ablation study on the BSDS500 test set.** We compare the components in our proposed framework, which includes both the learned affinities from the DAL network and the HERS algorithm.

tion and is therefore parameter-free. Whereas the balancing term in ERS plays a crucial role in avoiding extremely unbalanced superpixels.

By comparing DAL-HERS (cyan) with DAL-ERS (pink), we can see that the former enjoys much higher EV and BR scores at the cost of a lower ASA score. This trade-off can be explained by the fact that the superpixels produced by HERS are highly adaptive, i.e. *it keeps large homogeneous regions of an image intact whilst over-segmenting the texture-rich regions*. Adaptive superpixels are arguably more desirable than superpixels whose sizes are agnostic to the semantics of the image. However such adaptive behaviour has certain implications on the performance measures. Since the superpixels produced by HERS adhere strongly to the object boundaries and preserves the homogeneous regions, it is to be expected that it enjoys very good EV and BR scores. However, having adaptive superpixels also means that a small “leakage” in the boundary adherence would incur a big under-segmentation error, which negatively correlates with the ASA score.

**Benefit of external edge information.** For the purpose of achieving a higher ASA score, we could compromise a small amount of the performance gain in terms of EV and BR scores. The ASA score can be improved by strengthening the adherence to object boundaries given by the ground truth segmentations. Therefore, we additionally divide the edge weight by HED edge probabilities, which corresponds to DAL-HERS (HED) in Figure 5. As a result, we observe a notable increase in the ASA score of DAL-HERS (HED) as compared to that of DAL-HERS. The gain in the ASA score comes at a small cost of the EV and BR scores. This is again to be expected, because highlighting more boundary pixels would inevitably increase the false positives of boundary pixels thus decrease the BR and EV scores.

## 4.2. Comparison to State-of-the-Art Techniques

In this section, we compare our proposed method to various state-of-the-art classical and deep learning methods.

**Quantitative performance.** Figure 6 shows the quantitative comparison across all methods on both the BSDS500 and the NYUv2 test set. We include both DAL-HERS and DAL-HERS (HED) in the comparison, and refer to them as Ours and Ours (HED) for short. It can be seen that Ours outperforms all other competing methods in terms of EV and BR scores on both datasets. This means that the superpixels generated by our method fully captures the semantically homogeneous regions of images, and at the same time strongly adheres to the object boundaries (see Figure 4). Due to the highly adaptive nature of our superpixels, it does not lead to a high ASA score by design. The ASA score measures the overlap between the computed superpixels with the ground truth, where the ground truth labels are provided for object detection or semantic segmentation. As such, they do not delineate the fine details that our method captures so well, which results in the relatively low ASA score. To mitigate this, we could further incorporate HED edge information (as is explained in the ablation study). As a result, Ours (HED) achieves competitive performance against the majority of the superpixel methods that are being compared to.

**Qualitative performance.** In addition to the quantitative advantages exhibited by our proposed schemes, additional advantages can be demonstrated via visual comparisons of the segmentation results. In Figure 4, we observe several advantages of our method over the compared ones. Firstly, our technique prevents the over-segmentation of homogeneous regions in the scene. Clear examples of this effect can be seen in the grass on the first row, the sky on the second row, and the walls on the third and fourth rows. In all images, our method preserves fine details on the objects by focusing on rich-structure parts rather than uniform regions. Secondly, our technique displays the best boundary adherence. That is, our technique is able to better capture the object structures well. Examples of this property can be found by inspecting the zoomed-in views of the book and chair on the third and fourth rows. We provide further visual comparisons in the supplementary material.

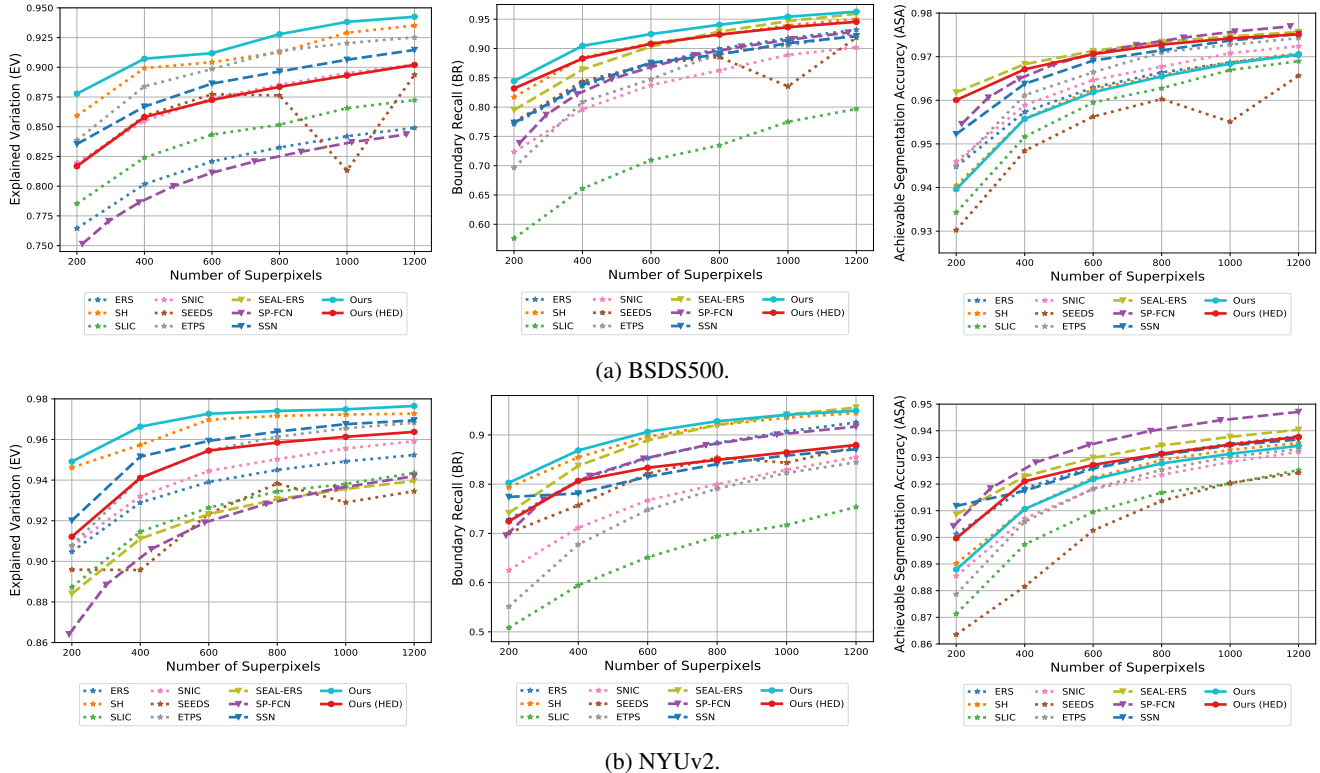


Figure 6: Comparison of our approach (solid lines) against the state-of-the-art of classical approaches (dotted lines) and deep learning based approaches (dashed lines) for superpixels. The performance of various methods are evaluated using EV, BR and ASA scores over different numbers of superpixels.

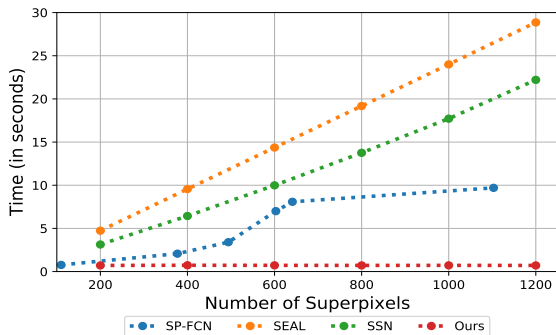


Figure 7: Cumulative runtime (in seconds) comparison of our proposed method against existing deep learning methods for computing 200 to 1200 superpixels averaged over 20 images in the BSDS500 dataset.

**Computational efficiency.** Another highly desirable property of any superpixel technique, as a stand-alone pre-processing tool, is the computational efficiency. We report the runtime (in seconds) of our proposed method and various deep learning based methods in Figure 7. To highlight the advantage of the hierarchical structure of HERS, we report the cumulative runtime of each method for computing various numbers of superpixels. For example, the time comparison at 400 on the  $x$ -axis reports the time that a method requires to produce both 200 and 400 superpixels.

It is notable that the runtime of our method is constant regardless of the various numbers of superpixels required by the user. This is because HERS constructs a hierarchical tree structure from which any number of superpixels can be extracted instantaneously, whereas all other methods have to run several times for each specified number of superpixels. It is also worth noting that SP-FCN cannot produce the exact user-specified number of superpixels, as it needs to partition an image into a number of regularly sized grid cells first. As such, we report the runtimes of the closest superpixel numbers it can obtain. Overall, our method provides a substantial decrease in computational time, independently of the number of superpixels, than the compared deep learning techniques. This makes our model a perfect fit to be used in any subsequent task.

## 5. Conclusion & Future Work

In this paper, we present a graph-based framework which consists of a neural network for obtaining deeply learned affinities, and an efficient superpixel segmentation method for producing highly adaptive superpixels. As demonstrated through experimental results, our proposed scheme compares favourably against state-of-the-art classical and deep learning based methods. Moreover, contrary to existing deep learning methods demanding linear time with respect



to the different numbers of user-specified superpixels, our technique exhibits constant time which make it feasible to be used as a preprocessing tool.

Future work might include tailoring our method to various computer vision tasks such as semantic segmentation, saliency detection, and stereo matching. In addition, it would be interesting to combine our deeply learned affinities with other graph-based superpixel methods.

## Acknowledgements

HP acknowledges the financial support by Aviva Plc. AIAR gratefully acknowledges the financial support of the CMIH and CCIMI University of Cambridge. CBS acknowledges support from the Philip Leverhulme Prize, the Royal Society Wolfson Fellowship, the EPSRC grants EP/S026045/1 and EP/T003553/1, EP/N014588/1, EP/T017961/1, the Wellcome Innovator Award RG98755, the Leverhulme Trust project Unveiling the invisible, the European Union Horizon 2020 research and innovation programme under the Marie Skłodowska-Curie grant agreement No. 777826 NoMADS, the Cantab Capital Institute for the Mathematics of Information and the Alan Turing Institute.

## References

- [1] Radhakrishna Achanta, Appu Shaji, Kevin Smith, Aurelien Lucchi, Pascal Fua, and Sabine Süsstrunk. SLIC superpixels compared to state-of-the-art superpixel methods. *IEEE Transactions on Pattern Analysis and Machine Intelligence*, 34(11):2274–2282, 2012.
- [2] Radhakrishna Achanta and Sabine Susstrunk. Superpixels and polygons using simple non-iterative clustering. In *Proceedings of the IEEE Conference on Computer Vision and Pattern Recognition*, pages 4651–4660, 2017.
- [3] Pablo Arbelaez, Michael Maire, Charless Fowlkes, and Jitendra Malik. Contour detection and hierarchical image segmentation. *IEEE Transactions on Pattern Analysis and Machine Intelligence*, 33(5):898–916, 2010.
- [4] Wanda Benesova and Michal Kottman. Fast superpixel segmentation using morphological processing. In *Conference on Machine Vision and Machine Learning*, pages 67–1, 2014.
- [5] Leyuan Fang, Shutao Li, Xudong Kang, and Jon Atli Benediktsson. Spectral–spatial classification of hyperspectral images with a superpixel-based discriminative sparse model. *IEEE Transactions on Geoscience and Remote Sensing*, 53(8):4186–4201, 2015.
- [6] Pedro F Felzenszwalb and Daniel P Huttenlocher. Efficient graph-based image segmentation. *International Journal of Computer Vision*, 59(2):167–181, 2004.
- [7] Huazhu Fu, Xiaochun Cao, Dai Tang, Yahong Han, and Dong Xu. Regularity preserved superpixels and supervoxels. *IEEE Transactions on Multimedia*, 16(4):1165–1175, 2014.
- [8] Raghudeep Gadde, Varun Jampani, Martin Kiefel, Daniel Kappler, and Peter V Gehler. Superpixel convolutional networks using bilateral inceptions. In *Proceedings of the European Conference on Computer Vision*, pages 597–613. Springer, 2016.
- [9] Josep M Gonfaus, Xavier Boix, Joost Van de Weijer, Andrew D Bagdanov, Joan Serrat, and Jordi Gonzalez. Harmony potentials for joint classification and segmentation. In *2010 IEEE computer society conference on computer vision and pattern recognition*, pages 3280–3287, 2010.
- [10] Leo Grady. Random walks for image segmentation. *IEEE transactions on pattern analysis and machine intelligence*, 28(11):1768–1783, 2006.
- [11] Kaiming He, Xiangyu Zhang, Shaoqing Ren, and Jian Sun. Deep residual learning for image recognition. In *Proceedings of the IEEE Conference on Computer Vision and Pattern Recognition*, pages 770–778, 2016.
- [12] Ahmad Humayun, Fuxin Li, and James M Rehg. The middle child problem: Revisiting parametric min-cut and seeds for object proposals. In *Proceedings of the IEEE International Conference on Computer Vision*, pages 1600–1608, 2015.
- [13] Varun Jampani, Deqing Sun, Ming-Yu Liu, Ming-Hsuan Yang, and Jan Kautz. Superpixel sampling networks. In *Proceedings of the European Conference on Computer Vision*, pages 352–368, 2018.
- [14] Diederik P Kingma and Jimmy Ba. Adam: A method for stochastic optimization. *arXiv preprint arXiv:1412.6980*, 2014.
- [15] Suha Kwak, Seunghoon Hong, and Bohyung Han. Weakly supervised semantic segmentation using superpixel pooling network. In *Proceedings of the AAAI Conference on Artificial Intelligence*, volume 1, page 2, 2017.
- [16] Alex Levinshstein, Adrian Stere, Kiriakos N Kutulakos, David J Fleet, Sven J Dickinson, and Kaleem Siddiqi. TurboPixels: Fast superpixels using geometric flows. *IEEE Transactions on Pattern Analysis and Machine Intelligence*, 31(12):2290–2297, 2009.
- [17] Zhengqin Li and Jiansheng Chen. Superpixel segmentation using linear spectral clustering. In *Proceedings of the IEEE Conference on Computer Vision and Pattern Recognition*, pages 1356–1363, 2015.
- [18] Zhenguo Li, Xiao-Ming Wu, and Shih-Fu Chang. Segmentation using superpixels: A bipartite graph partitioning approach. In *2012 IEEE conference on com-*

- puter vision and pattern recognition, pages 789–796, 2012.
- [19] Ming-Yu Liu, Oncel Tuzel, Srikumar Ramalingam, and Rama Chellappa. Entropy rate superpixel segmentation. In *Proceedings of the IEEE Conference on Computer Vision and Pattern Recognition*, pages 2097–2104. IEEE, 2011.
- [20] Pengpeng Liu, Michael Lyu, Irwin King, and Jia Xu. Selfflow: Self-supervised learning of optical flow. In *Proceedings of the IEEE/CVF Conference on Computer Vision and Pattern Recognition*, pages 4571–4580, 2019.
- [21] Yong-Jin Liu, Cheng-Chi Yu, Min-Jing Yu, and Ying He. Manifold SLIC: A fast method to compute content-sensitive superpixels. In *Proceedings of the IEEE Conference on Computer Vision and Pattern Recognition*, pages 651–659, 2016.
- [22] Vaia Machairas, Matthieu Faessel, David Cárdenas-Peña, Théodore Chabardes, Thomas Walter, and Etienne Decencière. Waterpixels. *IEEE Transactions on Image Processing*, 24(11):3707–3716, 2015.
- [23] Georg Maierhofer, Daniel Heydecker, Angelica I Aviles-Rivero, Samar M Alsaleh, and Carola-Bibiane Schönlieb. Peekaboo - Where are the objects? Structure adjusting superpixels. In *Proceedings of the IEEE International Conference on Image Processing*, pages 3693–3697. IEEE, 2018.
- [24] David R Martin, Charless C Fowlkes, and Jitendra Malik. Learning to detect natural image boundaries using local brightness, color, and texture cues. *IEEE Transactions on Pattern Analysis and Machine Intelligence*, 26(5):530–549, 2004.
- [25] Moritz Menze and Andreas Geiger. Object scene flow for autonomous vehicles. In *Proceedings of the IEEE conference on computer vision and pattern recognition*, pages 3061–3070, 2015.
- [26] Alastair P Moore, Simon JD Prince, Jonathan Warrell, Umar Mohammed, and Graham Jones. Superpixel lattices. In *2008 IEEE Conference on Computer Vision and Pattern Recognition*, pages 1–8. IEEE, 2008.
- [27] George L Nemhauser, Laurence A Wolsey, and Marshall L Fisher. An analysis of approximations for maximizing submodular set functions—i. *Mathematical programming*, 14(1):265–294, 1978.
- [28] Xiaofeng Ren and Jitendra Malik. Learning a classification model for segmentation. In *Proceedings of the IEEE International Conference on Computer Vision*, pages 10–17, 2003.
- [29] Philip Sellars, Angelica I Aviles-Rivero, and Carola-Bibiane Schönlieb. Superpixel contracted graph-based learning for hyperspectral image classification. *IEEE Transactions on Geoscience and Remote Sensing*, 58(6):4180–4193, 2020.
- [30] Jianbing Shen, Yunfan Du, Wenguan Wang, and Xuelong Li. Lazy random walks for superpixel segmentation. *IEEE Transactions on Image Processing*, 23(4):1451–1462, 2014.
- [31] Nathan Silberman, Derek Hoiem, Pushmeet Kohli, and Rob Fergus. Indoor segmentation and support inference from RGBD images. In *European Conference on Computer Vision*, pages 746–760. Springer, 2012.
- [32] Teppei Suzuki, Shuichi Akizuki, Naoki Kato, and Yoshimitsu Aoki. Superpixel convolution for segmentation. In *Proceedings of the IEEE International Conference on Image Processing*, pages 3249–3253. IEEE, 2018.
- [33] Dai Tang, Huazhu Fu, and Xiaochun Cao. Topology preserved regular superpixel. In *2012 IEEE International Conference on Multimedia and Expo*, pages 765–768. IEEE, 2012.
- [34] Wei-Chih Tu, Ming-Yu Liu, Varun Jampani, Deqing Sun, Shao-Yi Chien, Ming-Hsuan Yang, and Jan Kautz. Learning superpixels with segmentation-aware affinity loss. In *Proceedings of the IEEE Conference on Computer Vision and Pattern Recognition*, pages 568–576, 2018.
- [35] Michael Van den Bergh, Xavier Boix, Gemma Roig, Benjamin de Capitani, and Luc Van Gool. SEEDS: Superpixels extracted via energy-driven sampling. In *Proceedings of the European Conference on Computer Vision*, pages 13–26. Springer, 2012.
- [36] Andrea Vedaldi and Stefano Soatto. Quick shift and kernel methods for mode seeking. In *European Conference on Computer Vision*, pages 705–718. Springer, 2008.
- [37] Olga Veksler, Yuri Boykov, and Paria Mehrani. Superpixels and supervoxels in an energy optimization framework. In *European conference on Computer vision*, pages 211–224, 2010.
- [38] Shu Wang, Huchuan Lu, Fan Yang, and Ming-Hsuan Yang. Superpixel tracking. In *Proceedings of the IEEE International Conference on Computer Vision*, pages 1323–1330, 2011.
- [39] Xing Wei, Qingxiong Yang, Yihong Gong, Narendra Ahuja, and Ming-Hsuan Yang. Superpixel hierarchy. *IEEE Transactions on Image Processing*, 27(10):4838–4849, 2018.
- [40] Saining Xie and Zhuowen Tu. Holistically-nested edge detection. In *Proceedings of the IEEE International Conference on Computer Vision*, pages 1395–1403, 2015.

- [41] Fan Yang, Huchuan Lu, and Ming-Hsuan Yang. Robust superpixel tracking. *IEEE Transactions on Image Processing*, 23(4):1639–1651, 2014.
- [42] Fengting Yang, Qian Sun, Hailin Jin, and Zihan Zhou. Superpixel segmentation with fully convolutional networks. In *Proceedings of the IEEE Conference on Computer Vision and Pattern Recognition*, pages 13964–13973, 2020.
- [43] Jian Yao, Marko Boben, Sanja Fidler, and Raquel Urtasun. Real-time coarse-to-fine topologically preserving segmentation. In *Proceedings of the IEEE Conference on Computer Vision and Pattern Recognition*, pages 2947–2955, 2015.
- [44] Jianchao Zhang, Angelica I Aviles-Rivero, Daniel Heydecker, Xiaosheng Zhuang, Raymond Chan, and Carola-Bibiane Schönlieb. Dynamic spectral residual superpixels. *Pattern Recognition*, 112:107705, 2021.
- [45] Yuhang Zhang, Richard Hartley, John Mashford, and Stewart Burn. Superpixels via pseudo-boolean optimization. In *2011 International Conference on Computer Vision*, pages 1387–1394. IEEE, 2011.
- [46] Wei Zhao, Yi Fu, Xiaosong Wei, and Hai Wang. An improved image semantic segmentation method based on superpixels and conditional random fields. *Applied Sciences*, 8(5):837, 2018.

# Supplementary Materials for HERS Superpixels: Deep Affinity Learning for Hierarchical Entropy Rate Segmentation

## 6. Outline

This document extends the visual results and details presented in the main paper, which is structured as follows.

- Section 7: In the interest of completeness, we detail the definitions of the performance measures that are used in the main paper to evaluate the superpixel segmentation results of various methods.
- Section 8: We showcase various additional visual comparisons: i) demonstrating the advantage of our method against other state-of-the-art superpixel methods; and ii) showcasing the adaptiveness of our segmentation results with varying numbers of user-specified superpixel counts.

## 7. Performance Measures

The performance of various superpixel segmentation algorithms are commonly measured by the Under-segmentation Error (UE) [35], Achievable Segmentation Accuracy (ASA) [19] and Boundary Recall (BR) [24]. UE compares each computed superpixel with the ground truth superpixel that it overlaps with the most, and measures the “leakage” area that are not in the overlapped region. Opposite to UE, ASA quantifies the percentage of overlap between the segmented superpixels and the ground truth superpixels. That is, ASA can be directly obtained from UE as  $ASA=1-UE$ .

As such, we choose one out of these two and report ASA in our experiments. Concretely, ASA can be computed as

$$ASA(\mathcal{G}, \mathcal{L}) = \frac{1}{N} \sum_{k=1}^K \arg \max_{\mathcal{G}_c} |\mathcal{L}_k \cap \mathcal{G}_c|, \quad (7)$$

in which  $\mathcal{G} = \{\mathcal{G}_1, \dots, \mathcal{G}_C\}$  denotes the ground truth segmentation, and  $\mathcal{L} = \{\mathcal{L}_1, \dots, \mathcal{L}_K\}$  denotes the segmentation given by the chosen algorithm.

Boundary Recall (BR) measures the boundary adherence of the computed superpixels to the ground truth boundaries. It measures the proportion of ground truth boundary pixels that have been correctly identified by the computed superpixels. Concretely, BR can be computed as

$$BR(\mathcal{G}, \mathcal{L}) = \frac{TP(\mathcal{G}, \mathcal{L})}{TP(\mathcal{G}, \mathcal{L}) + FN(\mathcal{G}, \mathcal{L})}, \quad (8)$$

in which  $TP(\mathcal{G}, \mathcal{L})$  stands for true positive, it denotes the number of ground truth boundary pixels that have

been identified by the superpixel segmentation algorithm.  $FN(\mathcal{G}, \mathcal{L})$  stands for false negative, which denotes the remaining number of ground truth boundary pixels that have not been identified.

Additionally, we also report the Explained Variation (EV) [26] score, which quantifies the variance within an image that is captured by the superpixels without relying on any ground truth labelling. It is calculated using the following formula

$$EV(\mathcal{L}) = \frac{\sum_i (\mu_i - \mu)^2}{\sum_i (p_i - \mu)^2}, \quad (9)$$

where  $p_i$  denotes the RGB pixel values for the  $i$ -th pixel,  $\mu$  denotes the global mean of the RGB pixel values of an image, and  $\mu_i$  denotes the mean RGB pixel values for the superpixel that contains pixel  $p_i$ .

## 8. Supplementary Qualitative Results

In this section, we provide further visual comparisons on the BSDS500 [3] and NYUv2 [31] datasets across the following state-of-the-art techniques: i) classic techniques: ERS [19], SH [39], SLIC [1], SNIC [2], SEEDS [35], ETPS [43]; and ii) deep learning techniques: SSN [13], SEAL-ERS [34] and SP-FCN [42].

### 8.1. Additional visual comparisons with state-of-the-art methods

Figures 8 and 9 display two supplementary visual examples from the BSDS500 dataset. We note that amongst the compared techniques, our technique presents the most visually appealing output. By visual inspection, we can notice that our superpixels clearly shows better segmentations of fine details and stronger boundary adherence whilst avoiding partitioning homogeneous regions. In particular, several methods including the deep learning techniques of SEAL-ERS (see output (j)) and SP-FCN (see output (k)) often fail to capture the boundary structures. By contrast, our superpixels are better at capturing the objects of the scene including complex ones such as the shape of the flower and bird in Figures 8 and 9. Some examples of these advantages are highlighted in the zoomed-in views.

These benefits of our technique are also observed in indoors scenes as displayed in Figures 10 and 11, which are taken from the NYUv2 test set. We selected interesting samples with complex objects of varying sizes. In Figure 10, one can observe that none of the competing techniques are able to adhere well to the boundaries of small

objects (e.g. see the highlighted part in the blue zoomed-in square). This advantage of ours is expected since our technique avoids partitioning homogeneous areas (e.g, see the TV) and focuses on capturing the fine details in texture-rich scenes. This effect is even more noticeable in Figure 11, where our technique delineates the details of the main objects. Some highlighted cases can be seen in the zoomed-in views.

## 8.2. Various numbers of superpixels $K$

In this section, we demonstrate the adaptiveness of our superpixels with the number of user-defined superpixel counts ranging from 200 to 1200. Figures 12 and 13 showcase the results in terms of superpixel boundaries and in terms of the average RGB pixel features per superpixel on an image from the BSDS500 test set. It can be observed easily from the view with superpixel boundaries (see Figure 12) that our technique gradually focuses on segmenting the texture-rich regions of the image as the user-specified number of superpixels increases. As a result, our superpixels are able to provide a very accurate and smooth representation of the original image, even with a relatively small number of superpixels (see Figure 13).

Similarly, the same benefits of our superpixels can be observed in indoor scenes in Figures 14 and 15. We observe that our technique is able to delineate the main object boundaries in the image with 200 superpixels. With the increase of  $K$ , our technique further outlines the fine details within the identified objects. As a result, it is hard to even discern the difference visually between the original image (Figure 15 (a)) and the superpixel representations of the image (see Figure 15 (e) (f) (g)) at a first glance.

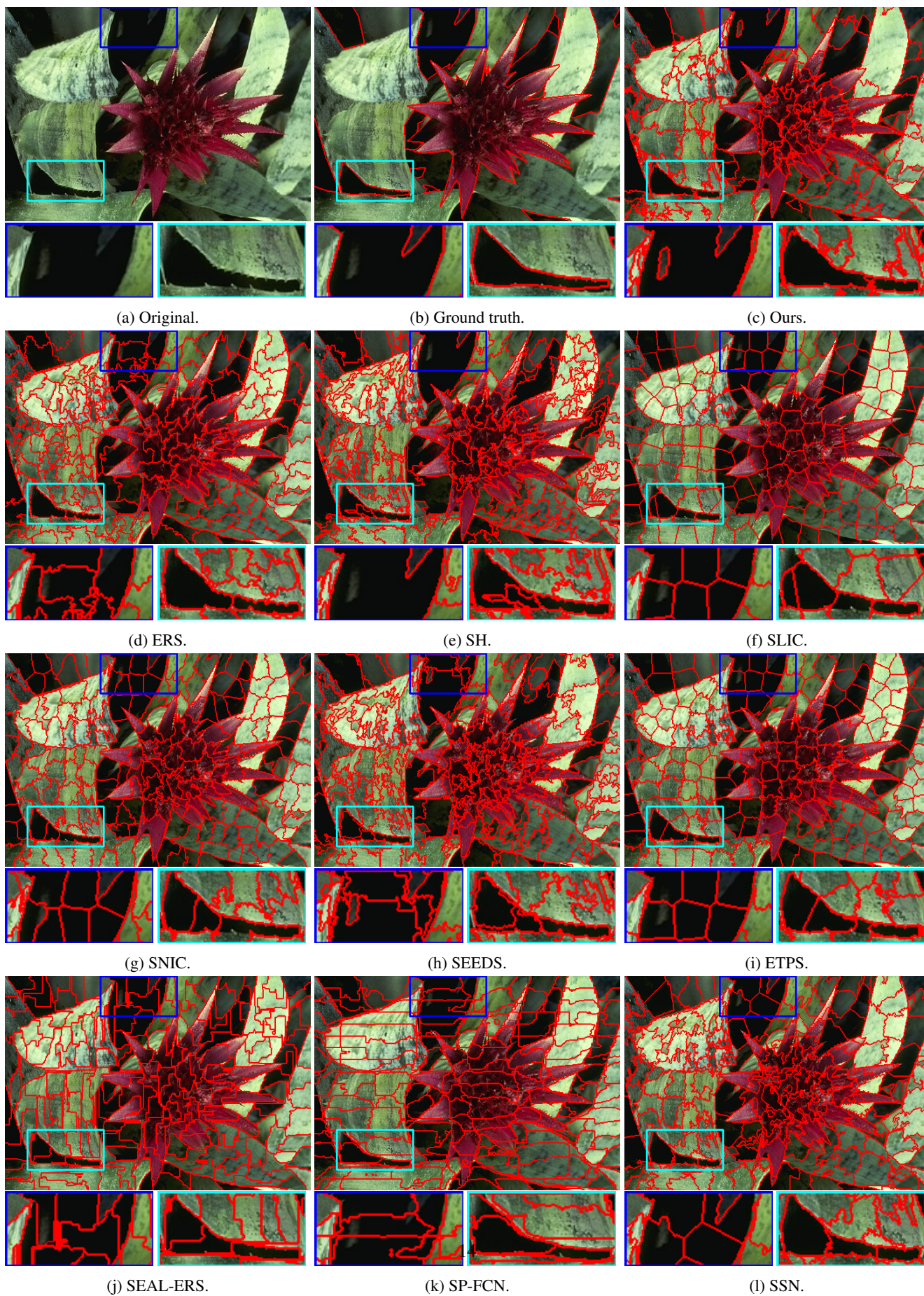
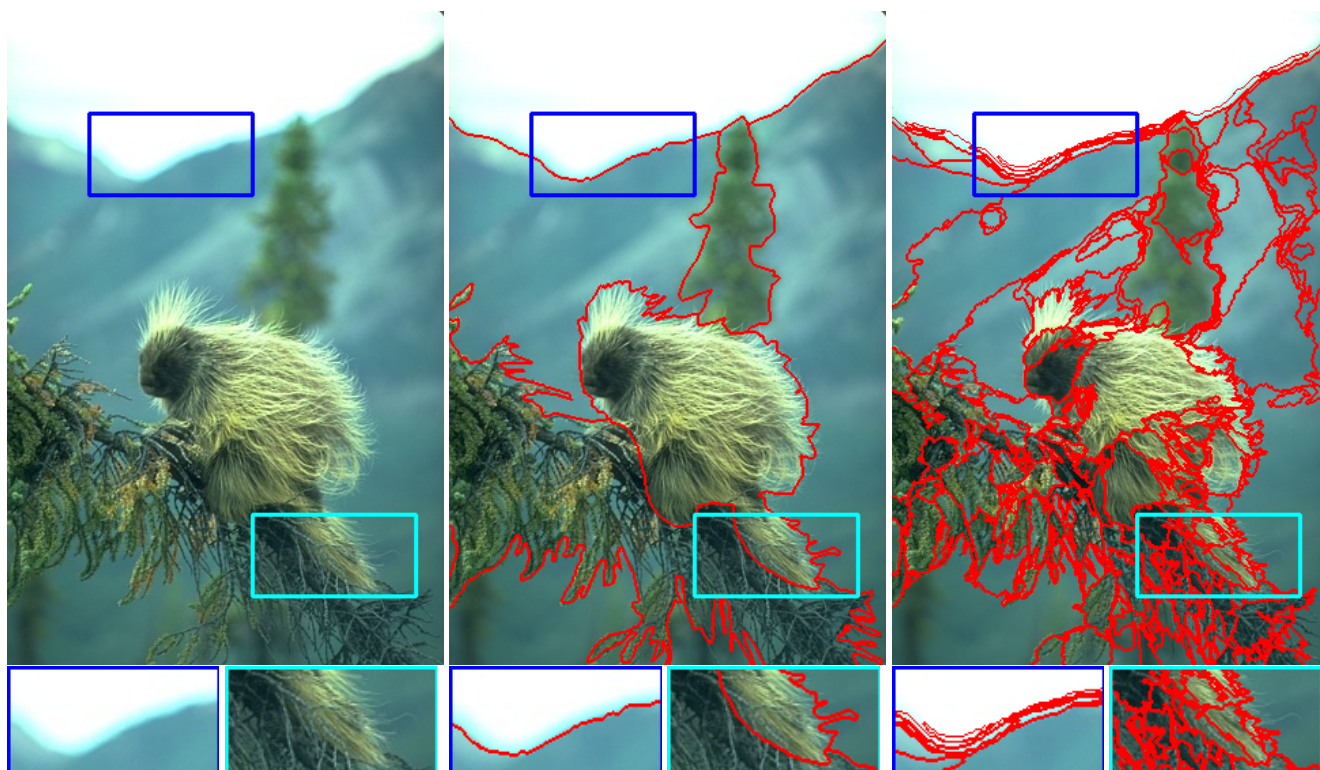


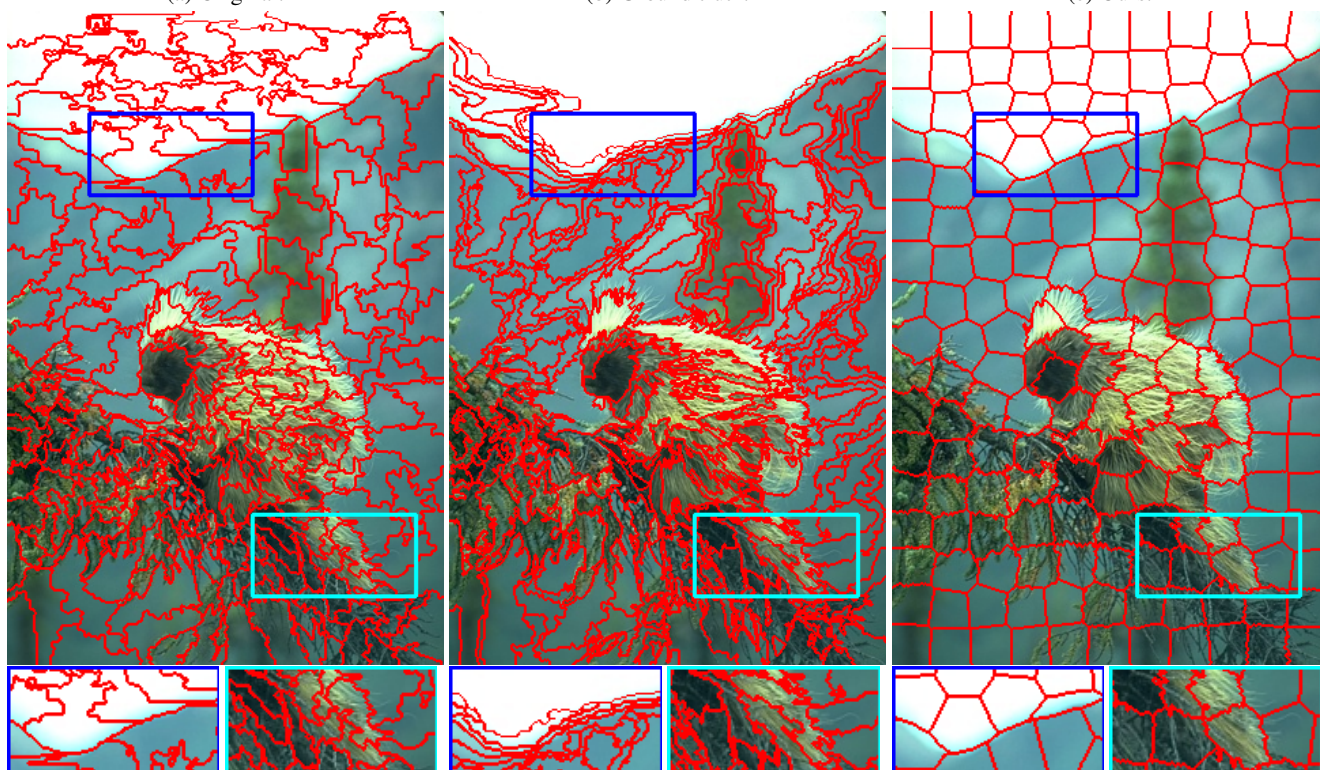
Figure 8: Segmentation results on a sample image from the BSDS500 test set with 200 superpixels.



(a) Original.

(b) Ground truth.

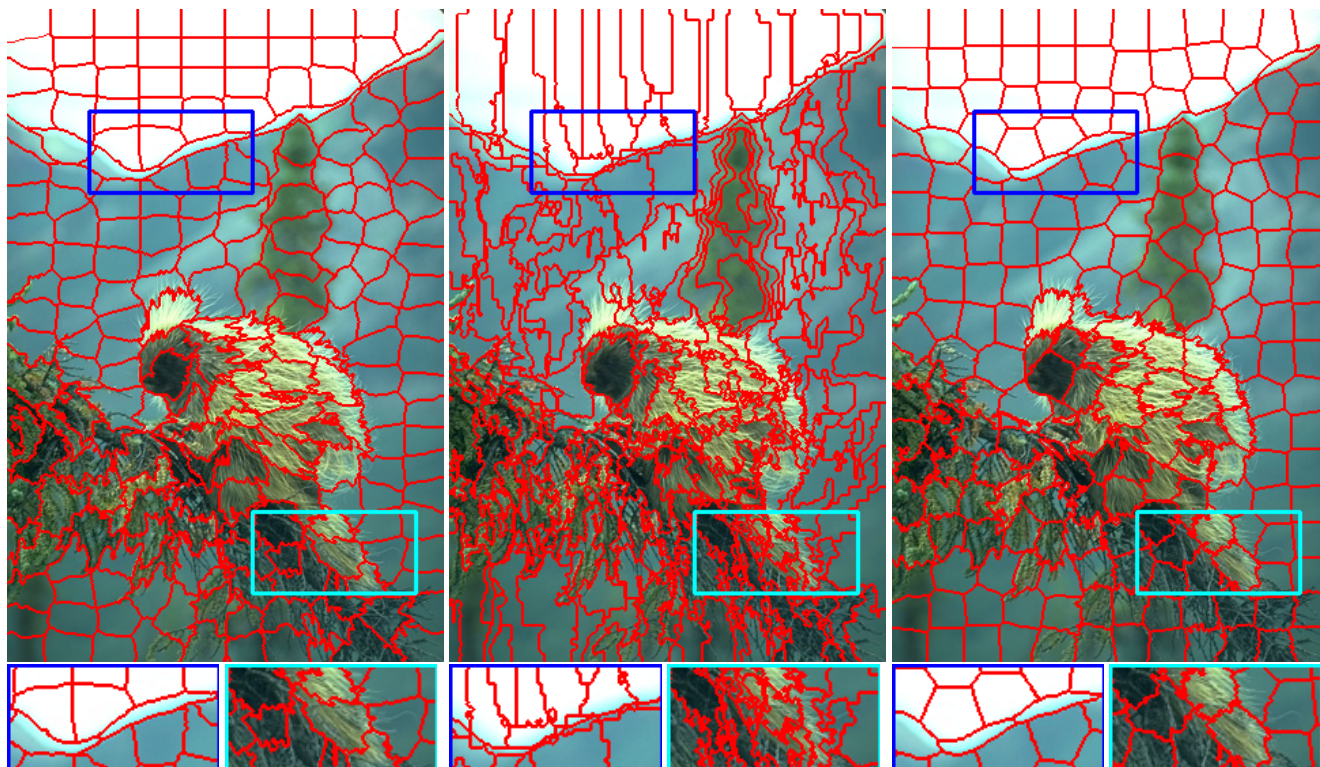
(c) Ours.



(d) ERS.

(e) SH.

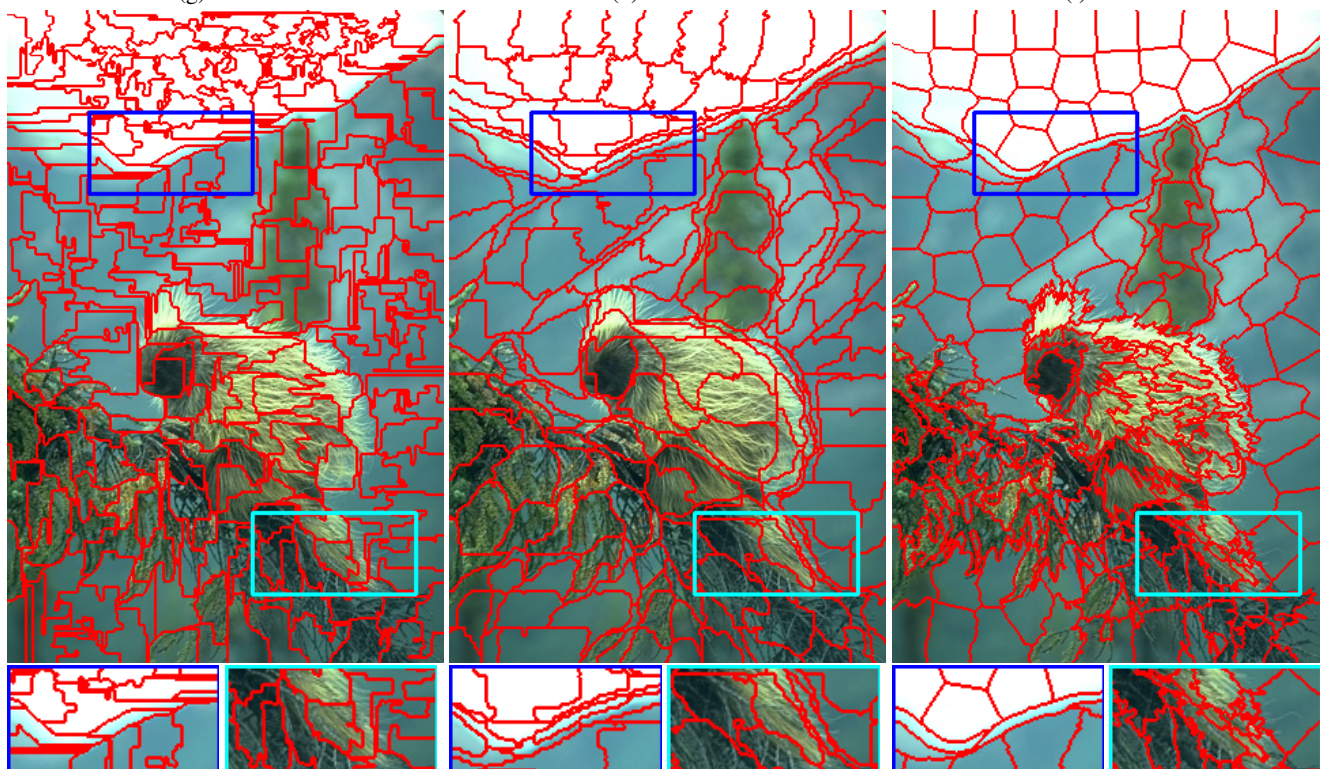
(f) SLIC.



(g) SNIC.

(h) SEEDS.

(i) ETPS.



(j) SEAL-ERS.

(k) SP-FCN.

(l) SSN.

Figure 9: Segmentation results on a sample image from the BSDS500 test set with 200 superpixels.





Figure 10: Segmentation results on a sample image from the NYUv2 test set with 200 superpixels.

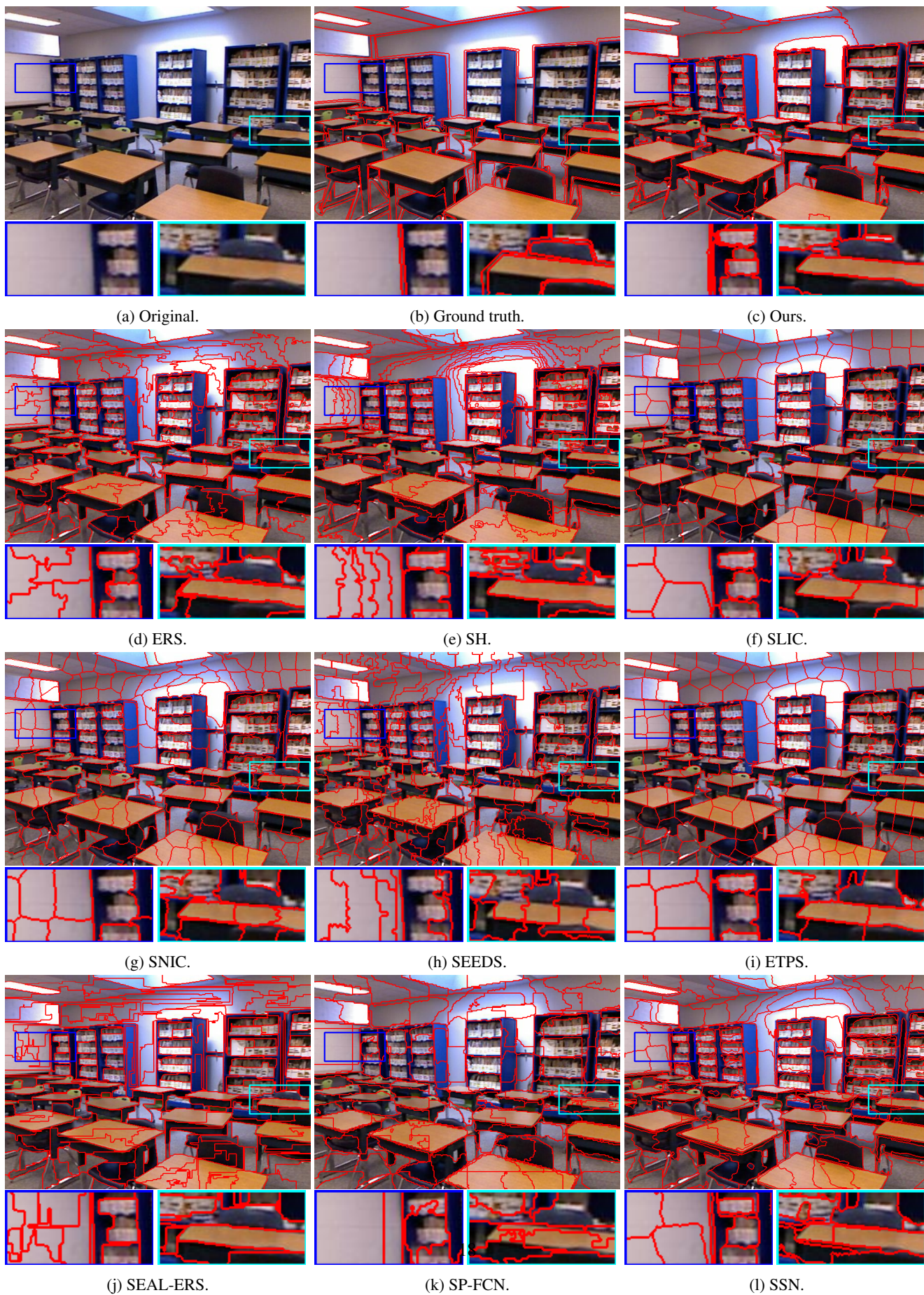


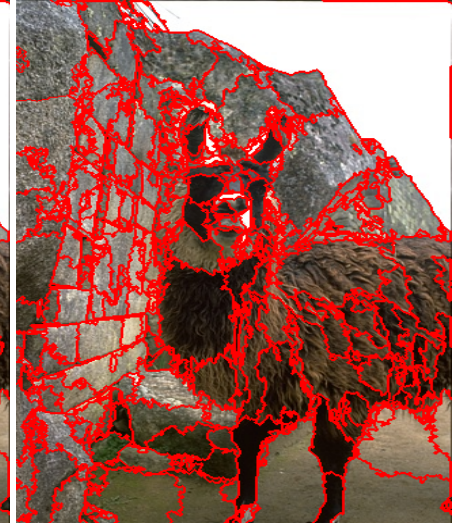
Figure 11: Segmentation results on a sample image from the NYUv2 test set with 200 superpixels.



(a) Original image.



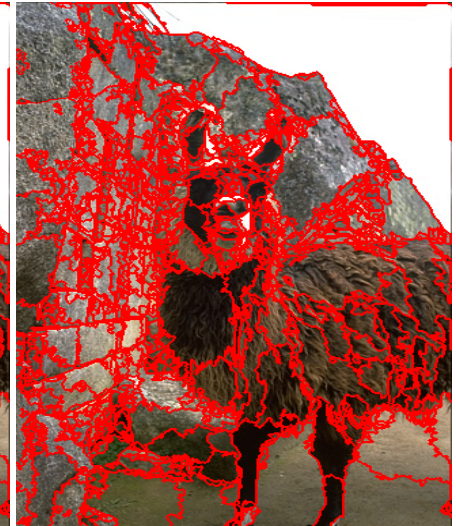
(b)  $K = 200$ .



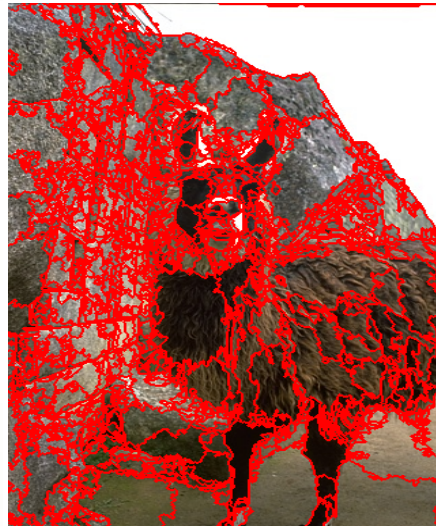
(c)  $K = 400$ .



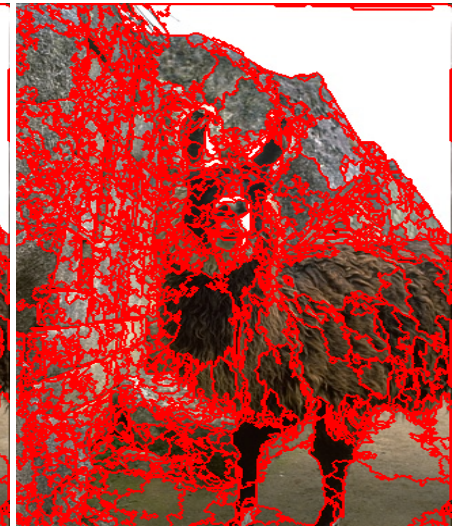
(d)  $K = 600$ .



(e)  $K = 800$ .



(f)  $K = 1000$ .



(g)  $K = 1200$ .

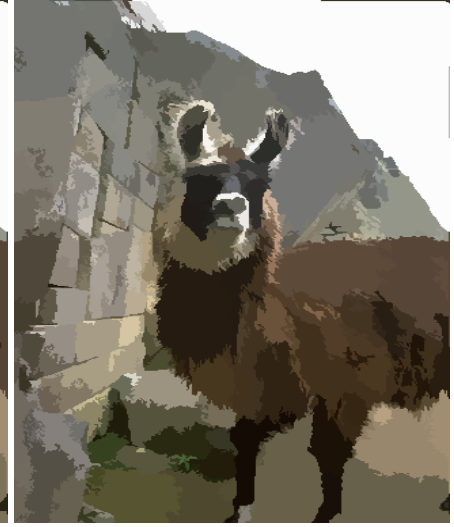
Figure 12: Segmentation results using our method on an image from the BSDS500 test set with varying number of superpixels.



(a) Original image.



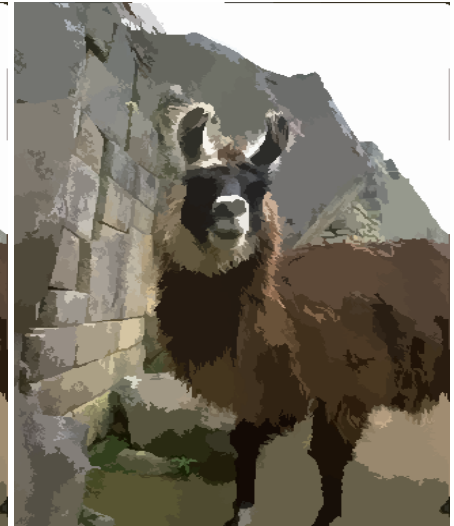
(b)  $K = 200$ .



(c)  $K = 400$ .



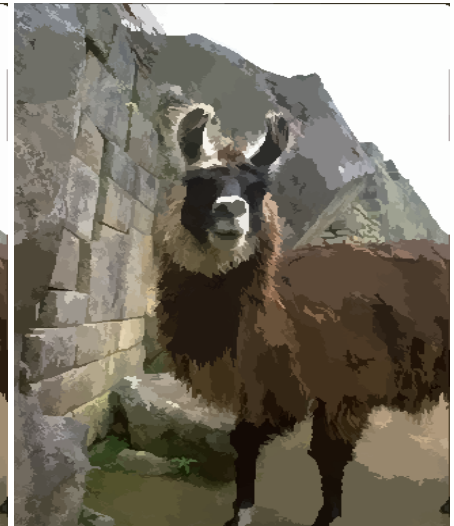
(d)  $K = 600$ .



(e)  $K = 800$ .



(f)  $K = 1000$ .



(g)  $K = 1200$ .

Figure 13: Segmentation results using our method on an image from the BSDS500 test set with varying number of superpixels. Each segmented image is represented with the average RGB pixel values of the corresponding superpixels.

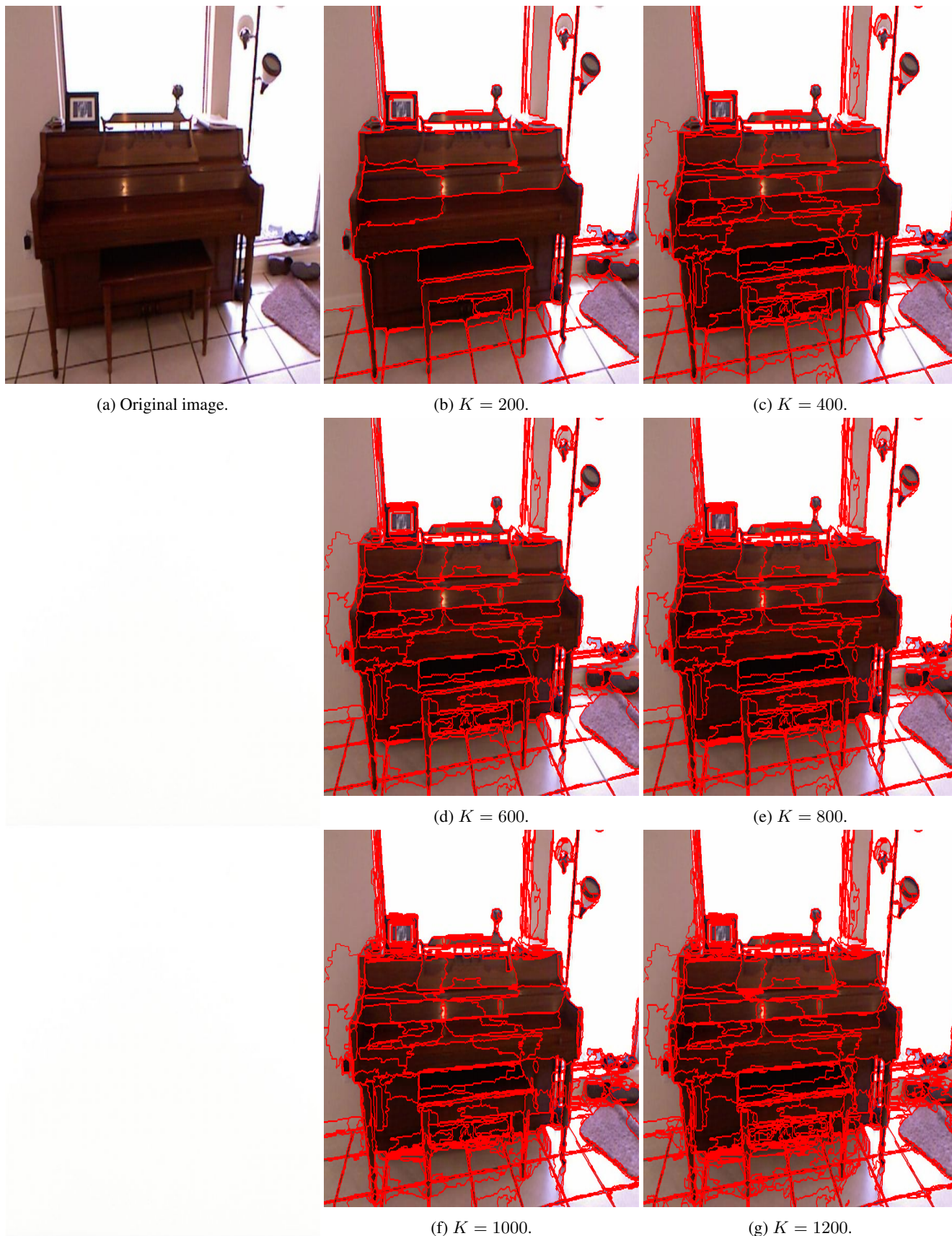
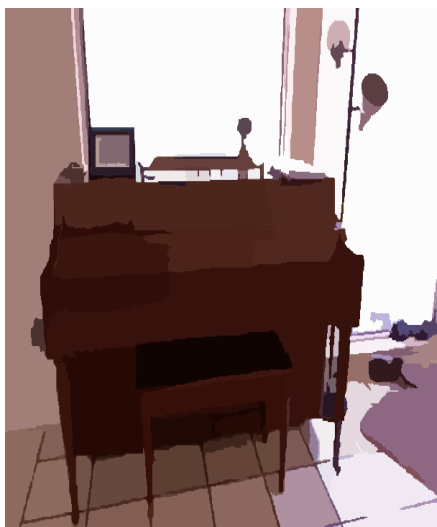


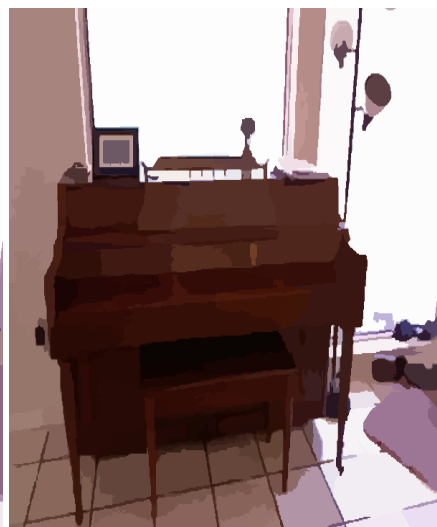
Figure 14: Segmentation results using our method on an image from the NYUv2 test set with varying number of superpixels.



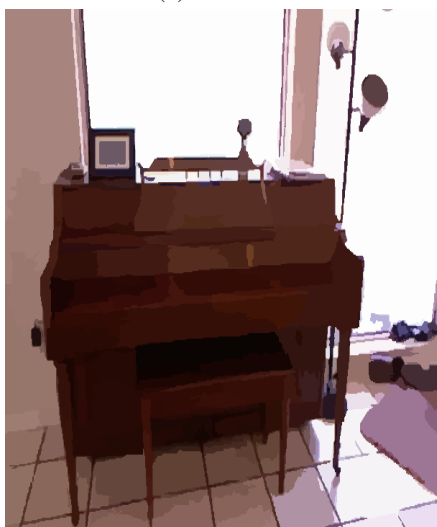
(a) Original image.



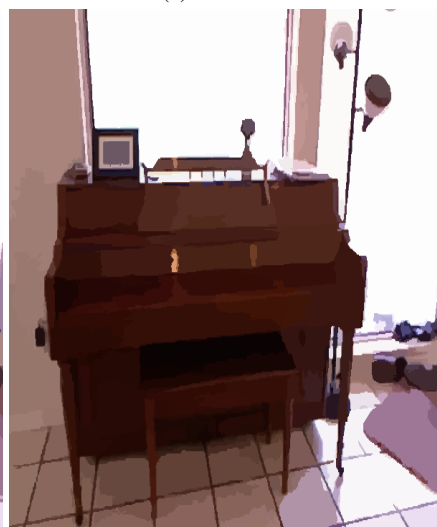
(b)  $K = 200$ .



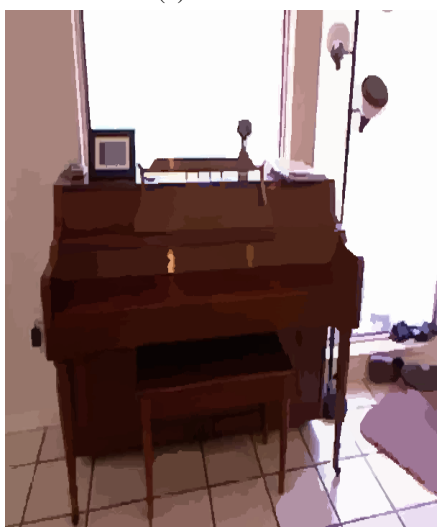
(c)  $K = 400$ .



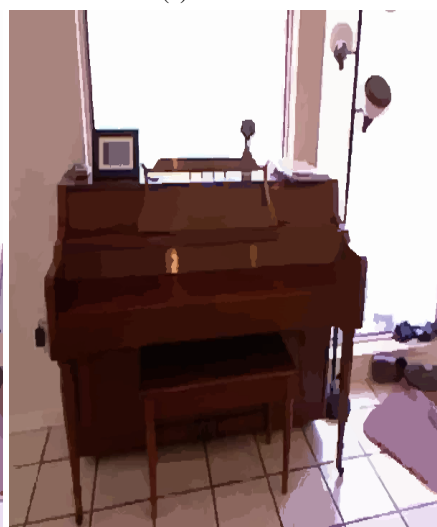
(d)  $K = 600$ .



(e)  $K = 800$ .



(f)  $K = 1000$ .



(g)  $K = 1200$ .

Figure 15: Segmentation results using our method on an image from the BSDS500 test set with varying number of superpixels. Each segmented image is represented with the average RGB pixel values of the corresponding superpixel.